ISTITUTO NAZIONALE DI FISICA NUCLEARE

Sezione di Perugia

INFN/AE–98/07
20 Aprile 1998

M.T. Brunetti, A. Codino:

CURVATURE MISIDENTIFICATION IN A MAGNET SPECTROMETER

Published by ***SIS–Pubblicazioni***
Laboratori Nazionali di Frascati

INFN – Istituto Nazionale di Fisica Nucleare
Sezione di Perugia

INFN/AE–98/07
20 Aprile 1998

CURVATURE MISIDENTIFICATION IN A MAGNET SPECTROMETER

M. T. Brunetti and A. Codino

Dipartimento di Fisica dell'Università degli Studi di Perugia and
Istituto Nazionale di Fisica Nucleare, Sezione di Perugia, Italy

Abstract

The search for antimatter in the primary cosmic radiation demands the identification of negatively charged antinuclides in large event samples of positively charged nuclides, which form the vast majority of cosmic rays. Magnet spectrometers equipped with tracking systems are universally employed for the determination of the charge sign via the measurement of curvature if the arrival direction is known.

The causes that generate a charge sign misidentification in magnet spectrometers for space experiments are enumerated and discussed. Algorithms conceived to identify curvature misidentification are given and applied to cosmic helium data collected by a balloon-borne spectrometer operated at the top of the atmosphere.

Some specific classes of helium trajectories suffering elastic nuclear scattering in the spectrometer can mimic those of antihelium. The simulation of these events in the spectrometer indicates that the curvature misidentification probability is $1.75 \cdot 10^{-6}$ for momenta between 8 and 100 GeV/c. The identification and removal of these specific trajectories from the experimental helium sample decreases the curvature misidentification probability of the spectrometer of a factor of 3.2. The comparison of this result with the present best upper limits to the antinucleus-to-nucleus ratios, in the range of 10^{-5} and 10^{-6} depending on the rigidity interval explored, demonstrates the critical role played by the algorithms that discriminate the curvature sign in space spectrometers.

1. Introduction

Numerous instruments have been operated in the last 40 years for the quest of cosmic antinuclei in the primary cosmic radiation. These instruments are mostly composed of detectors usually employed in Nuclear and Particle Physics in the appropriate configurations. Superconducting magnet spectrometers equipped with multiwire proportional chambers (MWPCs), drift chambers or solid state strip detectors form the heart of such instruments since they determine the charge sign of cosmic rays.

The search for antinuclei in the primary cosmic radiation initiated in 1961 has not yet produced any evidence for antinuclei, but only upper limits to the antinucleus-to-nucleus flux ratios. The most stringent upper limits at 95% confidence level available at high rigidity are $2 \cdot 10^{-5}$ [1] and $8 \cdot 10^{-6}$ at rigidity as low as 1 GV/c [2]. The relevance of the rigidity interval for the quest of antinuclei is illustrated in another paper [3].

New generations of experiments with improved sensitivity will either detect cosmic antinuclei or provide more stringent upper limits, possibly in the range of 10^{-7} to 10^{-9}. In both cases, however, either a limited number of antinuclei or no events at all will be detected. In this situation, the evaluation of the number of background events is of fundamental importance. The curvature misidentification of positively charged nuclides that may appear as negatively charged antinuclides is the major source of background. This problem cannot be circumvented since the cosmic-ray flux of positively charged particles overwhelms that of negatively charged particles in any site of the Galaxy.

The critical role played by the study reported in this paper is vividly illustrated by the two measurements [4,5] of the antiproton-to-proton flux ratio in the primary cosmic radiation made with the same payload but with two different tracking systems of the same superconducting magnet. The first measurement of the antiproton flux made in 1984 [4] differs by a factor of 8 from the second measurement made in 1996 [5]. It is not unlikely that curvature misidentification of cosmic-ray protons may account for a part of the observed difference in the two measurements.

The outcome of antinuclei search has even more fundamental implications on our image of the Universe than that of antiproton flux measurements. Therefore, the evaluation of the curvature misidentification rate of antinuclei in spectrometers is an even more critical and fundamental research area.

This work deals with curvature misidentification in magnet spectrometers employed in cosmic-ray experiments in space and complements and completes a previous background study of the MASS spectrometer [6].

Positive curvature and positive deflection designate, respectively, the curvature and deflection of a genuine positively charged particle. Analogous definition is intended for negative curvature and negative deflection.

Calculations and data analysis presented in this paper are restricted to cosmic helium. The importance of searching for antihelium in the primary cosmic radiation is known [7]. The data sample used for the comparison with calculations has been collected by the MASS (Matter-Antimatter Superconducting Spectrometer) experiment during two balloon flights in Fort Sumner (New Mexico) in 1991 and 1993 and amounts to 76346 helium events.

The paper is structured as follows. The problem, the causes and the parameters that play a significant role in the curvature misidentification are dealt with in Section 2. The results of simulations of elastic nuclear scattering of helium in the MASS spectrometer giving rise to curvatures consistent with those of antihelium are reported in Section 3. Note that a misidentified sign of helium curvature results in a fake antihelium event. Consistency checks on the sign of curvature of 76346 cosmic helium tracks observed in the MASS spectrometer are presented and discussed in Section 4. The simulated distributions of important parameters specifying the helium trajectories are compared with those resulting from the analysis of experimental data in order to identify fake antihelium curvatures. In Section 5, the curvature misidentification probability of the MASS spectrometer is calculated. Finally, in Section 6, an important subsample of cosmic helium appearing in the spectrometer with negative curvatures and surviving the requirements of well-measured tracks is selected and discussed.

2. Statement of the problem

2.1 Trajectory and curvature determination

Assume a nuclide with electric charge Z and momentum p that impinges onto the top, horizontal face of a detector volume immersed in a magnetic field, as depicted in figure 1.

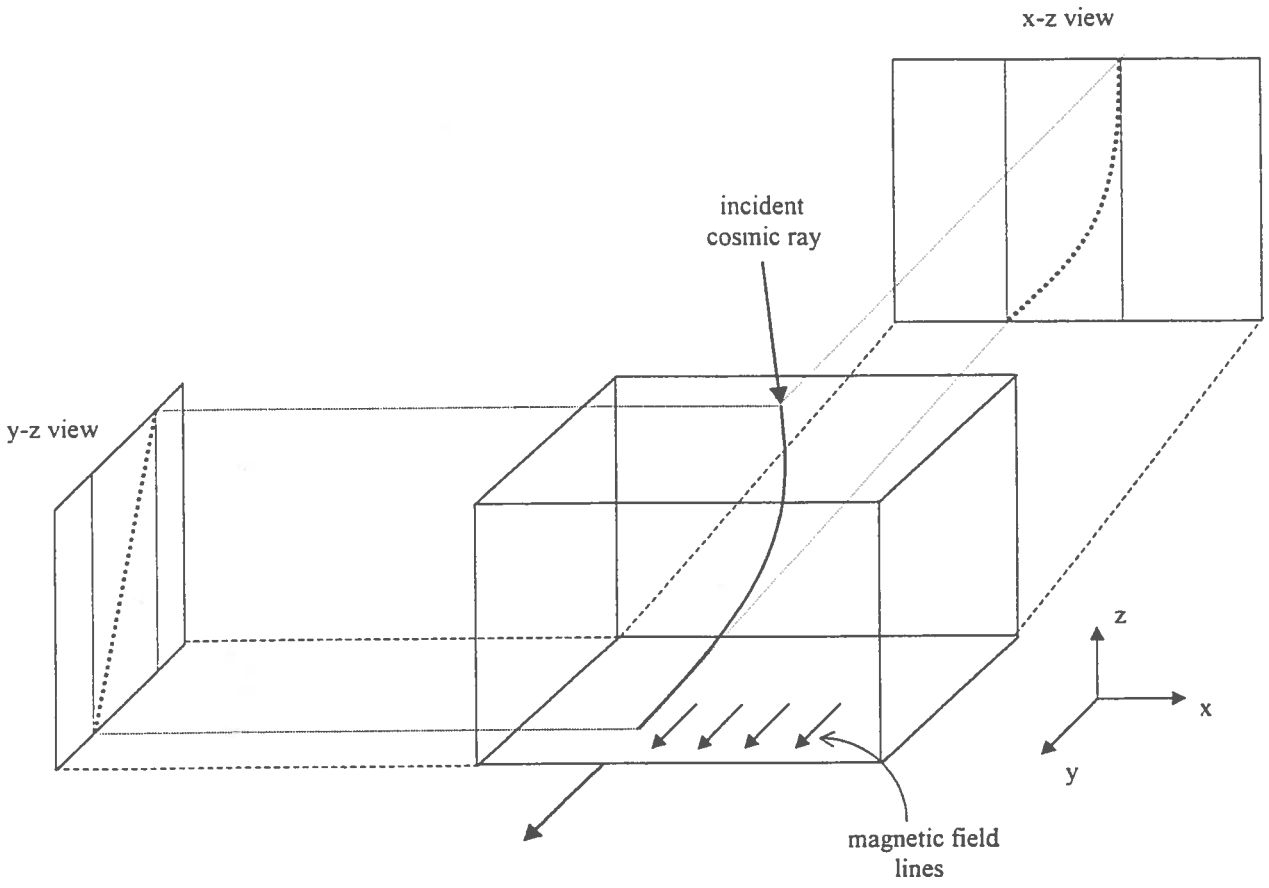

Figure 1. Trajectory projections of a charged particle penetrating a detector volume immersed in a uniform magnetic field. The projections are displayed in two perpendicular planes: the bending plane (x-z plane) and the non-bending plane (y-z plane). Multiwire proportional chambers, drift chambers or solid state strip detectors, can measure the trajectory projections.

Z is measured in units of the modulus of the electron charge (|e|) and B is the magnetic field strength. For sake of simplicity, consider a homogeneous magnetic field, constant in time and directed along the y-axis. Assume also that a set of plane drift chambers or other position detectors measure the coordinates of the incident particle in two perpendicular planes as shown, for example, in fig. 1. In this study, the notion of track is distinguished from that of the trajectory. The track is the set of coordinates resulting from measurements, while the trajectory is the corresponding curve in space reconstructed via appropriate algorithms applied to the set of measured coordinates and errors. The two projected trajectories are represented by the function $x \equiv f(z)$ in the x-z plane (bending plane in fig. 1) and $y \equiv g(z)$ in the y-z plane (non-bending plane). Let be x' and x'' the first and the second derivatives, respectively, to the projected trajectory in the point $x_1=f(z_1)$ and $y' \equiv dg/dz$, $y'' \equiv d^2g/dz^2$ those in the point $y_1=g(z_1)$. The tangent vector to an arbitrary point x_1, y_1, z_1 of the trajectory is denoted by $\vec{v}(x', y', 1)$.

The curvature, $\vec{c}$, at any space point x_1, y_1, z_1 is a vector normal to the curve in the specified point, given by:

$$\vec{c} = \left(\frac{x''}{v^2} - \frac{ax'}{v^4} \right) \vec{u}_x + \left(\frac{y''}{v^2} - \frac{ay'}{v^4} \right) \vec{u}_y - \left(\frac{a}{v^4} \right) \vec{u}_z \qquad (2)$$

where $a \equiv x' x'' + y' y''$, $v = +\sqrt{x'^2 + y'^2 + 1}$ is the modulus of the velocity and $\vec{u}_x$, $\vec{u}_y$, $\vec{u}_z$ are unit vectors along the orthogonal axes of the reference frame.

In the simple case of a homogeneous field *in vacuo*, the trajectory is a segment of a circle or a full circumference of radius ρ given by: $\rho = p/(B\, Z\, |e|)$. The modulus of the curvature, in this case $1/\rho$, may be determined by measuring the sagitta $s=\rho[1-\cos(L/2\rho)]$ where L is the length of the circumference segment. If $\rho >> L$, a condition usually fulfilled in many experiments, the following approximation may be used:

$$s \cong \frac{L^2}{8\rho} \qquad (3)$$

As apparent from equation (2), the measurement of the curvature sign requires the determination of the first and second derivatives of the projected trajectories (see Appendix B of ref. [6]).

The projected trajectories, represented by the functions f(z) and g(z), are commonly determined by the least square method. Let be X_m (n) and σ_x (n) the measured coordinates and errors, respectively, in the bending plane at the depth z (n), where n is the n-th position measurement. The track, represented here by the set of computed coordinates, X_t (n), is determined by the χ^2-minimization. In the x-view the χ^2_x is given by:

$$\chi^2_x = \sum_{n=1}^{N} \frac{[X_t(n) - X_m(n)]^2}{\sigma_x^2(n)}$$

where N is the number of position measurements of a given trajectory.

Thus, a result of the minimization algorithm is the set of N points X_t (n) giving the trajectory at various depths z (n). Note that the function x=f(z) is another representation, possibly analytical, of the N points X_t(n). An analogous minimization algorithm is valid for the y-view.

The track fitting determines the magnetic deflection or simply the deflection, η, defined as Z |e|/p and the deflection uncertainty σ_η, given by $\sigma_\eta = \left(\frac{d^2\chi^2}{d\eta^2} \right)^{-\frac{1}{2}}$ (see Appendix B of ref. [6]). Often, the rigidity, R, related to the deflection by the relation R=1/η is also used.

2.2 Error sources in curvature measurement

If the number of position measurements for trajectory reconstruction, N, is large enough and the position errors are sufficiently small, the curvature would be unambiguously determined for an arbitrary large number of incident particles. In practice, because of many instrumental effects and various types of scattering processes, curvature misidentification insidiously occurs in operational spectrometers.

Three distinct categories of phenomena induce curvature misidentification: (1) spurious position measurements of the projectile trajectory; (2) performance limitation of the spectrometer due to the bending power of the magnet, the number of position measurements, the position resolutions of the tracking system and similar parameters; (3) projectile scattering with matter in the spectrometer volume.

The first category includes position measurements generated by multiple tracks in the chambers, inelastic hadronic interactions, spurious signals close to the main track due to delta rays and electronic noise in various forms.

At large momentum values, close to the maximum detectable rigidity, curvature misidentification becomes a quite probable event even if the projectile does not undergo a significant scattering in the matter layers of the spectrometers. This occurs when the deflection becomes comparable to the position resolutions of the tracking system and represents the second category of errors.

The trajectories of nuclides with electric charge Z suffering peculiar scatterings can mimic those of antinuclides with opposite electric charge, -Z. Relevant scatterings with matter are due to two different processes: Coulomb scattering and elastic nuclear scattering. This third category of errors, unlike the previous two, is represented by events that fall into the optimum ranges of those parameters characterizing the spectrometer performance.

It follows that any given set of selection criteria conceived to identify cosmic antihelium applied to the raw data containing a large sample of helium events (for instance, 10^5 events) will also contain fake antihelium events because of curvature misidentification.

The curvature misidentification rate in spectrometers depends on a number of important parameters enumerated below. Parameters related to the nature of the incident particle are:

(1) the momentum;
(2) the arrival direction and impact coordinates on the sensitive volume of the spectrometer;
(3) the atomic number Z.

Other parameters related to the characteristics and performance of the detectors composing the spectrometer:

(4) the global matter thickness of the tracking system and its distribution in space;
(5) the bending power of the magnet along the particle trajectory, $\int \vec{B} \cdot d\vec{l}$;
(6) the total number of position measurements, N, and the spacing between the chamber planes;
(7) the position resolutions of the tracking system, σ_x (n) and σ_y (n) where n denotes the n-th measurement along the trajectory with $N_{min} \leq n \leq N_{max}$, where N_{min} is the minimum number

of position measurements required for the track fitting which is 3 and N_{max} is the maximum.

3. Computed probability of misidentifying helium curvatures

The purpose of this Section is to calculate the number of helium events (Z = +2) penetrating the tracking system of the MASS spectrometer appearing as antihelium events (Z = -2) because of the elastic nuclear scattering.

3.1 Elastic nuclear scattering and curvature misidentification

The hybrid chamber system used in the MASS-91 and MASS-93 flights incorporated in the simulation program is shown in figure 2 and is described elsewhere [6,8].

A cosmic-ray helium penetrating the chamber stack from above encounters 2 planes of MWPCs, the first drift chamber module, 3 planes of MWPCs, the second drift chamber module and finally, the last 3 planes of MWPCs. There is a maximum of 19 position measurements in the maximum bending plane and 11 in the orthogonal plane. Thus, $N_{max}(x)=19$ and $N_{max}(y)=11$. Most of the helium events have typical values in the range 9-13 for N(x) and 9-11 for N(y).

The total matter thickness of the tracking system of the spectrometer amounts to 0.55 g/cm^2.

The total and differential cross sections for nuclear interactions of helium with the target nuclei in the chambers have been taken from the available experimental data [9-12].

Curvature misidentification becomes a probable event in the MASS spectrometer (like in other magnet spectrometers) if the following four conditions are met:

(1) Particle scattering takes place in the sensitive volume of the tracking system (see figures 1, 3 and 4).

(2) The direction of motion after the scattering must be contained in the appropriate space sector in such a way that the curvature sign of the second segment of the trajectory (SK in fig. 3) is opposite to that determined by the first segment of the trajectory (segment PS in fig. 3).

(3) The scattering angle should be sufficiently large to generate a change in the particle direction, so that the probability of having a curvature sign of the full trajectory opposite to those of the two trajectory segments is a likely event.

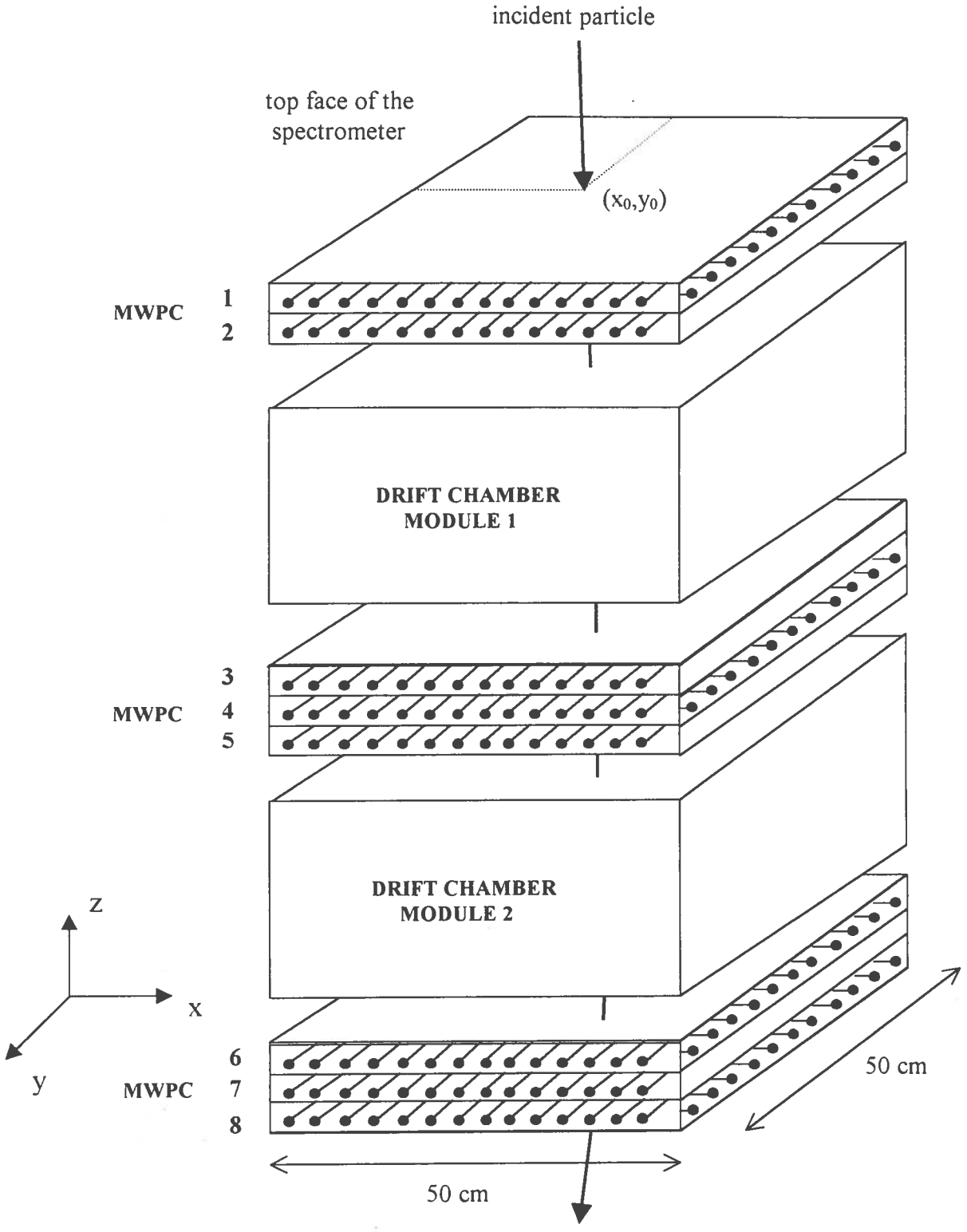

Figure 2. Multiwire proportional chambers (MWPCs) and drift chambers forming the tracking system of the MASS spectrometer dedicated to the antiproton, positron and antihelium search in the primary cosmic radiation. The distance between chambers, the position resolution, the number of chamber planes, the total matter thickness of the tracking system and the magnet bending power are the five basic parameters playing a salient role in the curvature misidentification.

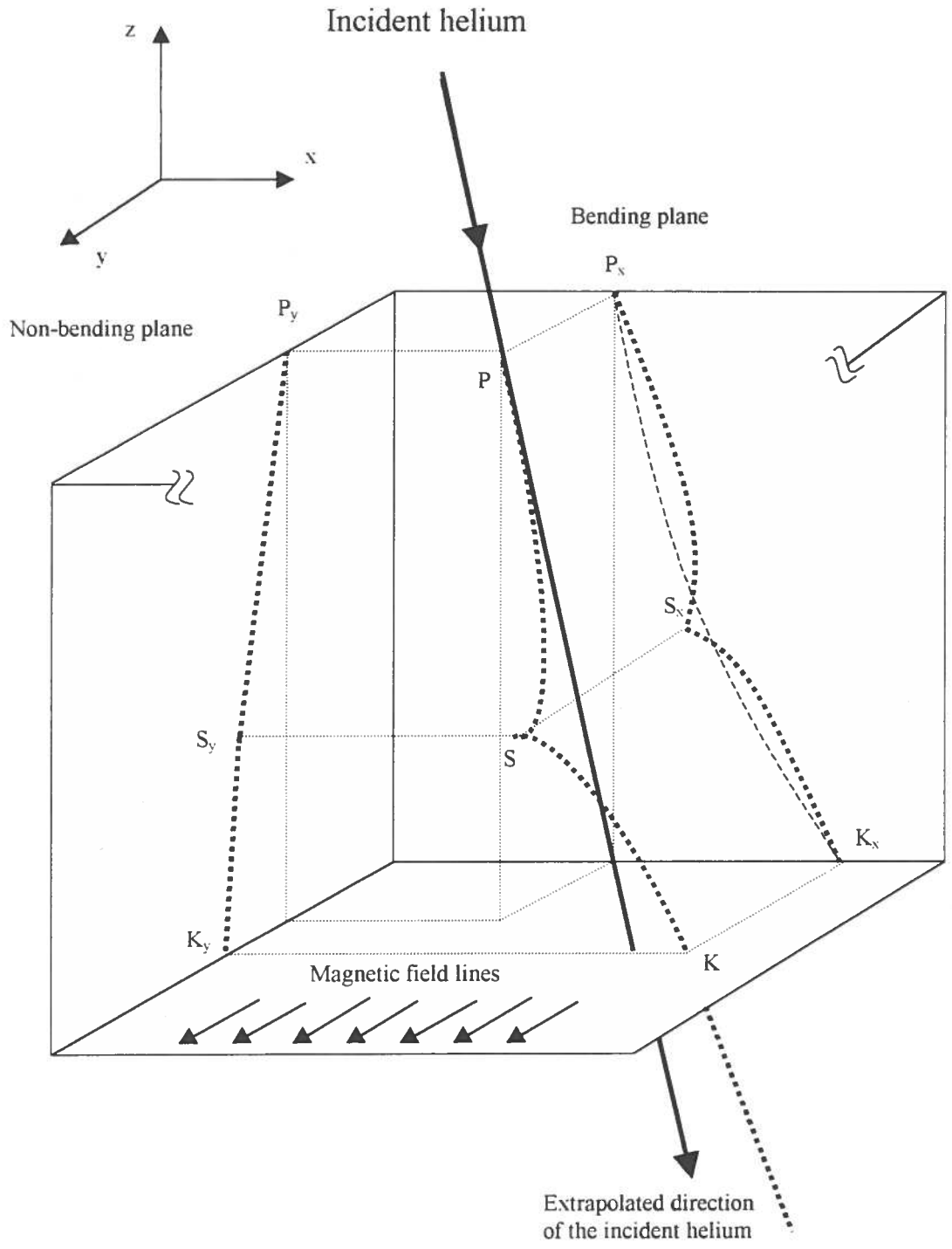

Figure 3. Qualitative illustration of the misidentification of the curvature sign of a cosmic ray penetrating the sensitive volume of a typical magnet spectrometer. The dotted lines in the x-z and y-z planes represent the position measurements. The dashed curve in the x-z view is the reconstructed trajectory resulting by the interpolation of the position measurements (for simplicity the corresponding curve in the y-z view has been omitted). At the point S an elastic nuclear scattering occurs. In some cases, as the one depicted here, the projected trajectory, P_xK_x (dashed line), resulting from the interpolation algorithms has a curvature sign opposite to those of the two curve segments, P_xS_x and S_xK_x (dotted lines) of the same trajectory.

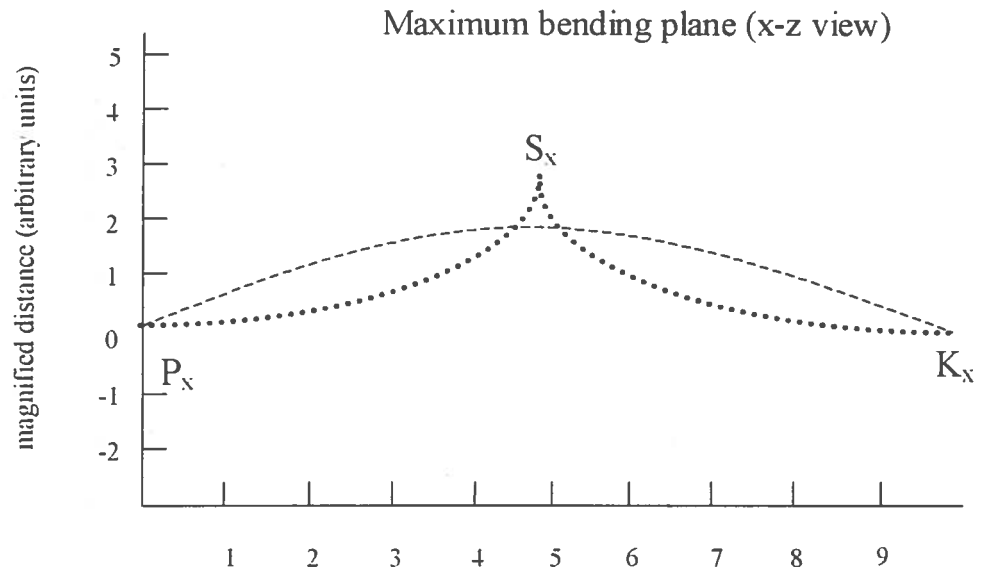

Figure 4-a

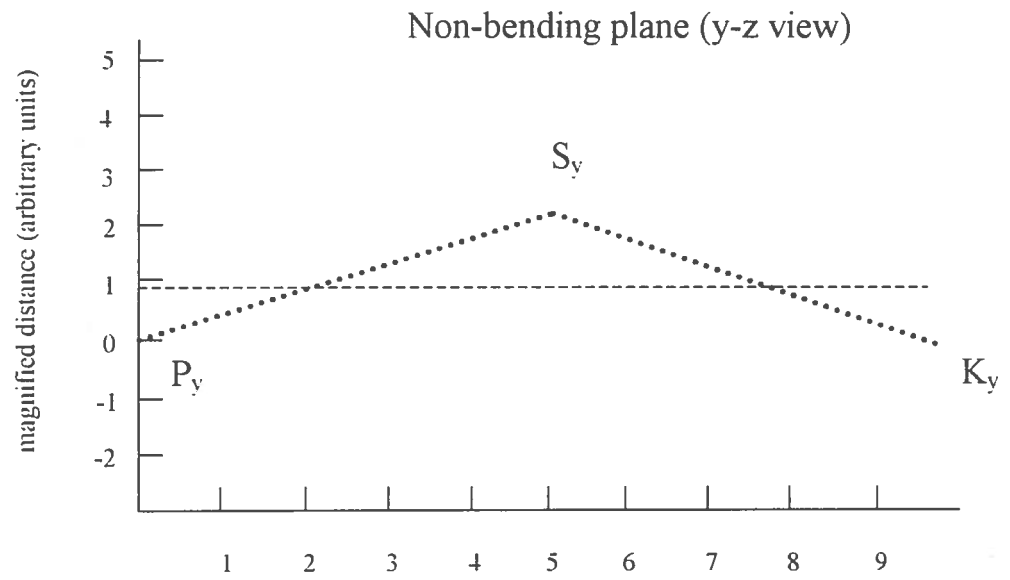

Figure 4-b

Figure 4. Qualitative illustration of the two projected trajectories of a cosmic-ray helium suffering an elastic nuclear scattering in S (see also fig. 3).

(4-a) The first trajectory segment in the x-z plane, P_x S_x, and the second one, S_x K_x, represent the paths (dotted lines) of the cosmic ray in the chamber volume. The dashed curve represents the trajectory resulting by the interpolation algorithms applied to the position measurements; its curvature sign is opposite to those of the trajectory segments P_x S_x and S_x K_x (dotted lines).

(4-b) Paths (dotted curve) and reconstructed trajectory (dashed curve) in the y-z plane of the same cosmic ray displayed in figs. 4-a and 3.

(4) The χ^2-values in the two projections of the trajectory are less than 2.5. This value is dictated by the χ^2-distributions of typical tracks without scattering which are mostly populated at values below 2.5 (see the subsequent figure 7).

While the tracking system shown in fig. 2 is peculiar of the MASS spectrometer, the curvature misidentification process described above and the illustrations of figs. 1, 3 and 4 may also apply to other magnet spectrometers. It is useful to notice here that the bulk of helium events suffering elastic nuclear scatterings leading to incorrect curvature signs is routinely eliminated by the χ^2-cut. The problem faced in this study in its most critical aspect is the identification of those genuine helium events with negative deflection that survive the χ^2-cut.

3.2 Simulation of helium trajectories in the MASS spectrometer

The effects of the Coulomb scatterings in the MASS spectrometer contributing to the deflection uncertainty have been investigated by a sample of cosmic ground muons [6] and included, with the appropriate modifications for the helium projectile, in the simulation program. A sample of 100000 helium events suffering elastic nuclear scatterings in the tracking system of the spectrometer (biased sample) has been generated. This biased sample corresponds to an unbiased helium sample of $1.48^{+0.25}_{-0.18}\cdot 10^7$ events as it results from the total matter thickness of the spectrometer and the average elastic cross sections of helium with the target nuclei (C, O, Al, Ar, Cu and W). For the 3 most abundant target nuclei the cross sections for elastic nuclear scatterings are: 1120±310 mb (copper), 579^{+23}_{-31} mb (aluminum) and 325^{+5}_{-13} mb (carbon). Note that inelastic collisions of cosmic helium taking place in the tracking system are removed from the experimental data sample. Therefore, inelastic collisions are ignored in the simulation.

Significant experimental characteristics embedded in this simulation are:

(1) Uniform distribution of impact coordinates, x_0 and y_0, at the top face (see fig. 2) of the chamber system.

(2) Uniform distribution of arrival directions of the cosmic helium in the spectrometer acceptance (see fig. 2 of ref. 12). These arrival directions are specified by the tangents of

the helium trajectories in the two measuring planes, $(dx/dz)_0$ and $(dy/dz)_0$ at the points x_0 and y_0.

(3) Measurement errors for each position $\sigma_x(n)$ or $\sigma_y(n)$ consistent with space resolutions of the tracking system. The position resolutions of the MWPC in the maximum bending plane ranges from 180 μm to 270 μm and that in the y-z plane between 0.6 mm to 1.2 mm. The position resolutions of the drift chambers vary between 50 μm and 160 μm depending on the driftpath.

(4) The number of position measurements of the simulated track is sampled from the observed distribution of the number of position measurements determined during the flights.

(5) The track fitting in the magnetic field volume which provides the 5 classical input parameters x_0, y_0, $(dx/dz)_0$, $(dy/dz)_0$ and the deflection η.

Note that each simulated helium event has been treated with the same trajectory reconstruction procedure utilized for the experimental data.

3.3 Selection criteria in the MASS spectrometer

Three groups of selection criteria (or cuts) have been applied to both experimental and simulated helium events in the spectrometer; they are referred to as helium selection criteria, trajectory cuts and curvature cuts.

Helium events are selected in the rigidity interval $4 \leq R \leq 50$ GV/c, with pulse amplitude compatible with $|Z|=2$ and with arrival directions from the top to the bottom of the instrument implying $\beta>0$, where β is the particle velocity. The geometrical arrangement of the time-of-flight counter system is described elsewhere [13] and has an up-down discrimination of more than 30 standard deviations. This preliminary selection is denoted by helium selection criteria. More severe requirements on the helium trajectories are defined below and are referred to as trajectory cuts. A good-quality track in the spectrometer must satisfy the following set of inequalities.

(α) The values of the χ^2 distributions are in the ranges:

$\chi_x^2 \leq 2.5$, $\chi_y^2 \leq 2.5$.

Note that reduced χ^2 distributions are used in this study.

(β) The number of chambers in the x-z view, $N_{ch}(x)$ and that in the y-z view, $N_{ch}(y)$, providing position measurements utilized in trajectory determination are constrained by:
$N_{ch}(x) > 12$ and $N_{ch}(y) > 9$.

(γ) The deflection error distribution, σ_η, of the experimental data is bell-shaped with a tail at high values and a mean value of 0.01 c/GV. Good-quality tracks exhibit:
$\sigma_\eta \leq 0.0175$ c/GV.

(δ) The field integral of helium tracks in the spectrometer volume is constrained by the condition:
$\int B \cdot dl \geq 0.16$ Tesla·m.
The map of the magnetic field strength of the superconducting magnet is shown elsewhere (see fig. 1 of ref. [13]).

(ε) The relative accuracy in the deflection measurement satisfies:
$|\eta| / \sigma_\eta > 5$.

The criteria α, β, γ, δ and ε (trajectory cuts) for good-quality tracks, or looser versions of them, have been used in the data analysis of antiprotons [5], primary positrons [14], muons and pions [15] and atmospheric electrons and positrons [16].

3.4 Curvature misidentification probability of genuine cosmic helium

The deflection distribution of simulated helium events that have undergone elastic nuclear scattering has been calculated and is displayed in figure 5 in the negative deflection interval. It results that an average helium fraction of $1.14 \cdot 10^{-2}$ appears in the negative deflection band. When the trajectory cuts are applied to the simulated helium events an average decrease of a factor of 44 is observed. From this calculation one finds, on the average, that one fake antihelium is generated every $0.57 \cdot 10^6$ helium events because of elastic nuclear scattering in the spectrometer.

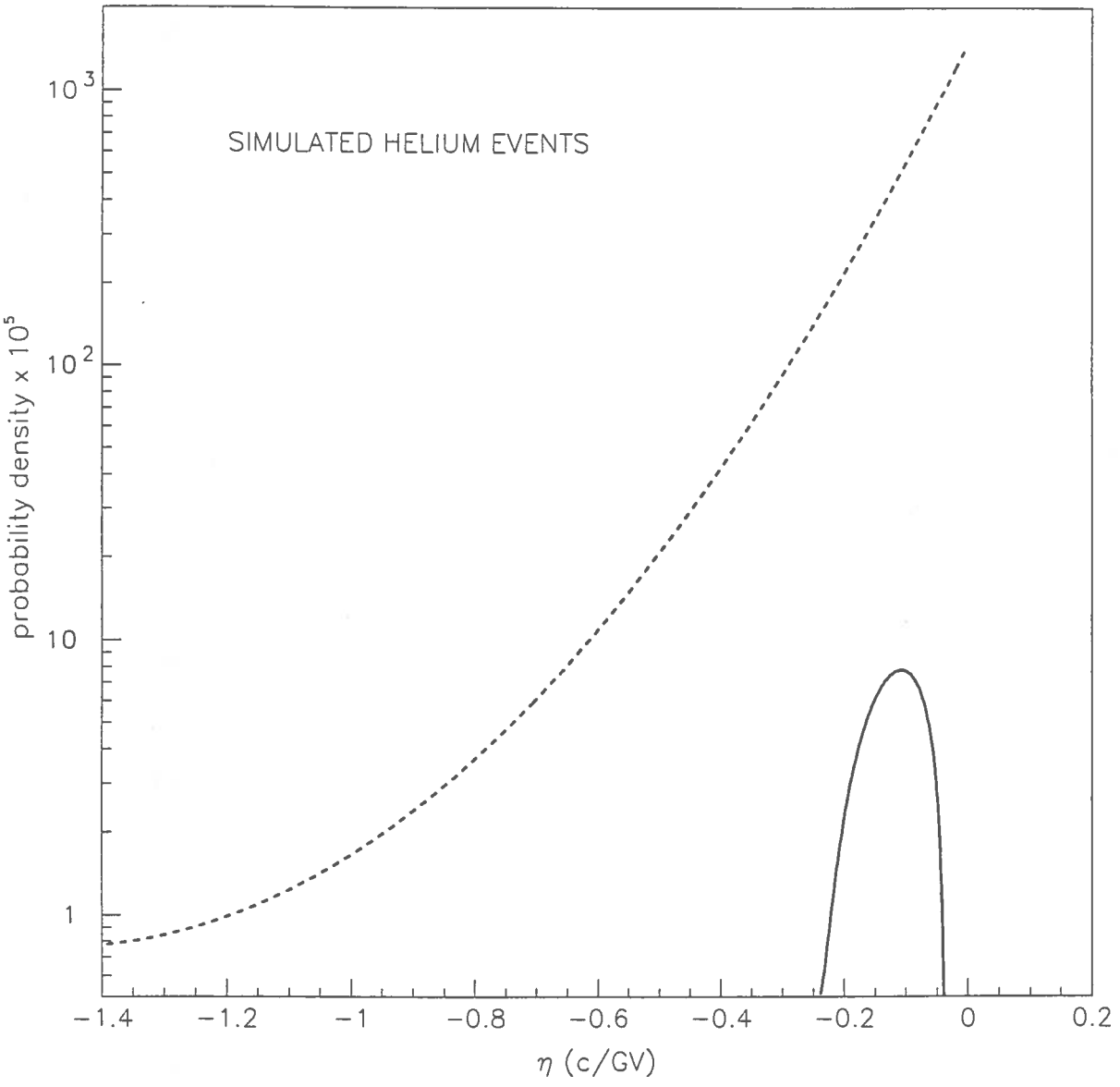

Figure 5. Computed deflection distribution in the negative deflection interval (dashed line) originated by genuine helium events in the momentum band 8-100 GeV/c. All these events have undergone elastic nuclear scatterings in the matter layers of the spectrometer. The corresponding distribution obtained by applying the trajectory cuts on the helium events represented by the dashed line is shown by a solid line. The depletion of events close to $\eta=0$ is due to the selected rigidity interval, $4 \leq R \leq 50$ GV/c which implies $0.02 \leq \eta \leq 0.25$.

This class of events, genuine helium appearing as fake antihelium, has specific properties investigated in the subsequent Sections 5 and 6 which permit one to reduce the fake antihelium contamination while preserving a high detection efficiency for genuine helium events.

All simulated events have been subdivided into two categories: (1) regular and (2) scattering events. The first category are events penetrating the spectrometer without suffering an elastic nuclear scattering. Events that have undergone elastic nuclear scatterings in the spectrometer volume (see figures 1 and 3) belong to the second category. Note that Coulomb scattering is included in the simulation of nuclear scattering events.

It is interesting to study the dependence of the number of fake antihelium events on the accuracy of the deflection measurements $|\eta|/\sigma_\eta$ both for scattering and regular events. Figure 6 shows $|\eta|/\sigma_\eta$ versus negative deflection for a simulated helium sample of 100000 events that suffer elastic nuclear scatterings. These events are not uniformly distributed in the variable $|\eta|/\sigma_\eta$ versus η, but populate the characteristic zone shown in fig. 6. Almost all the 200000 simulated regular events reported in the window populate a smaller negative deflection interval and have values of the quantity $|\eta|/\sigma_\eta$ well below the standard cut (ε).

4. Consistency checks of the curvature

A consistency check on the sign of curvature is given by the following technique. The full track length, s, characterized by the 4 parameters η, σ_η, χ_x^2 and χ_y^2 is subdivided into two equal segments, s_1 and s_2, such that $s_1 = s_2 = s/2$. Let be $\eta(1)$, $\sigma_\eta(1)$, $\chi_x^2(1)$, $\chi_y^2(1)$ the parameters defining the quality of the first segment and $\eta(2)$, $\sigma_\eta(2)$, $\chi_x^2(2)$, $\chi_y^2(2)$ those of the second segment.

Good χ^2 -values of any trajectory is a prerequisite for the other physical quantities found on the trajectory to be reliably computed. Accordingly, good-quality trajectories should exhibit the 6 χ^2-values consistent with statistical fluctuations typical of χ^2-distributions. Figure 7 shows the χ^2-distributions both for the full trajectory and the two segments for an experimental helium sample. The distribution of the difference in the χ^2-values $2\chi_x^2 - \chi_x^2(1) - \chi_x^2(2)$ is expected to have zero mean for well-measured helium tracks. Figure 8 shows this distribution for the x-view of the tracking system. A similar distribution of the quantity $2\chi_y^2 - \chi_y^2(1) - \chi_y^2(2)$ is obtained for the y-view.

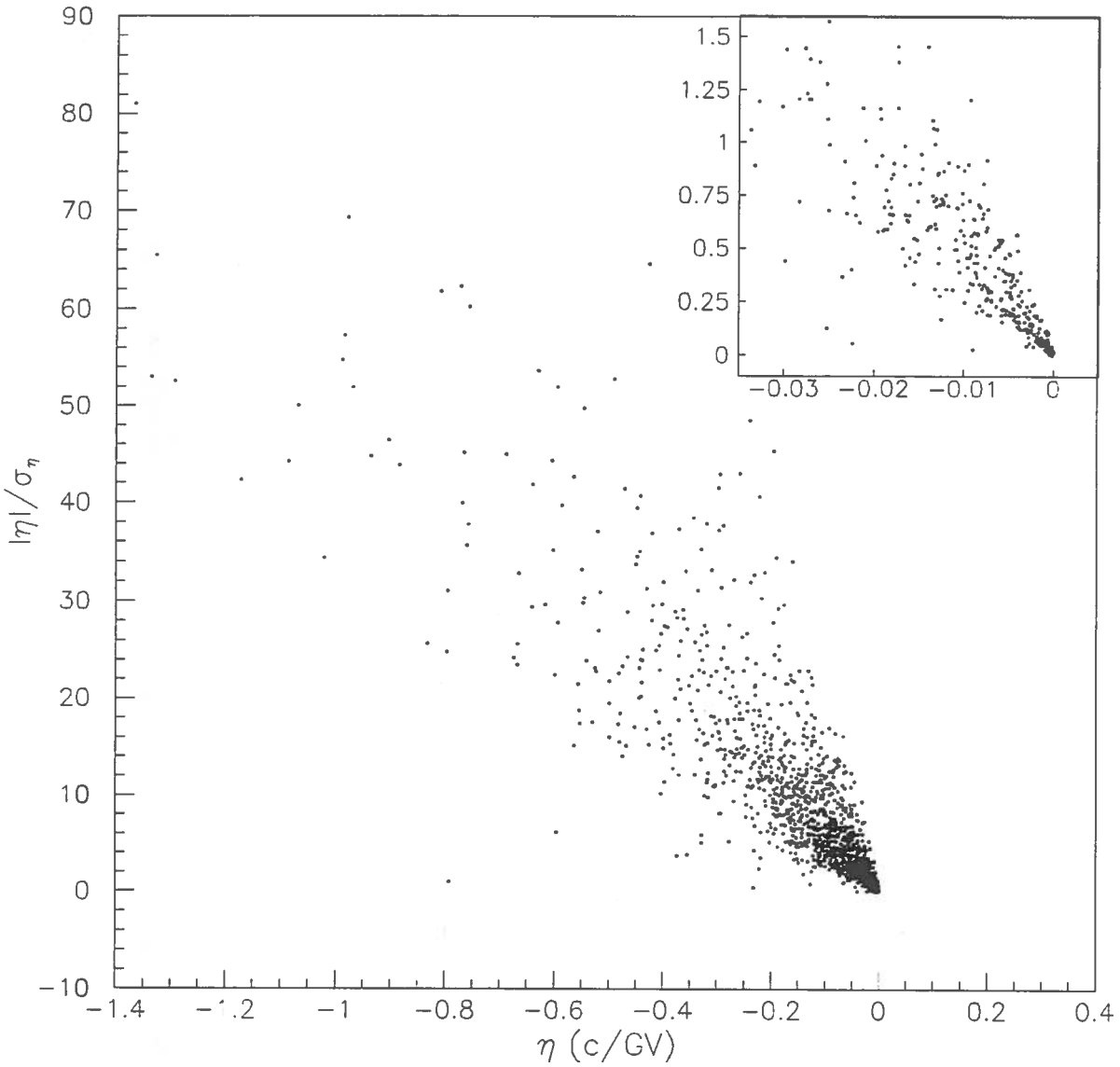

Figure 6. Deflection accuracy distribution versus negative deflection for a sample of 100000 helium events generated by the Monte Carlo method. The deflection accuracy is defined as $|\eta|/\sigma_\eta$. All these events have undergone an elastic nuclear scattering in the spectrometer. The small figure at the top right displays the corresponding bidimensional distribution for regular events i.e. those without elastic nuclear scattering.

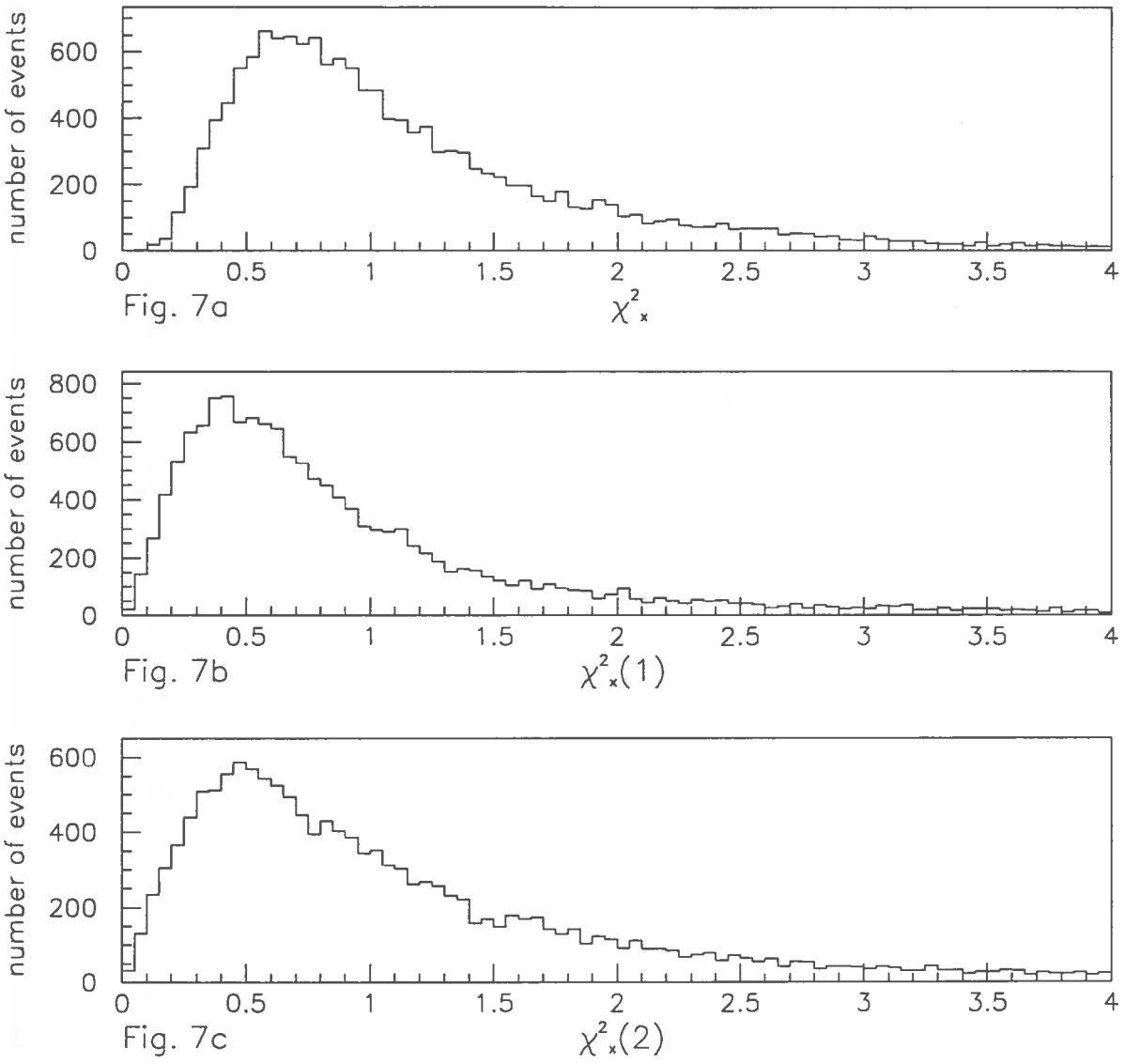

Figure 7. χ^2-distribution of a sample of 13947 events surviving the good-trajectory cuts in the MASS-91 flight for the full trajectory (7-a) and the two segments of the same trajectory (7-b and 7-c).

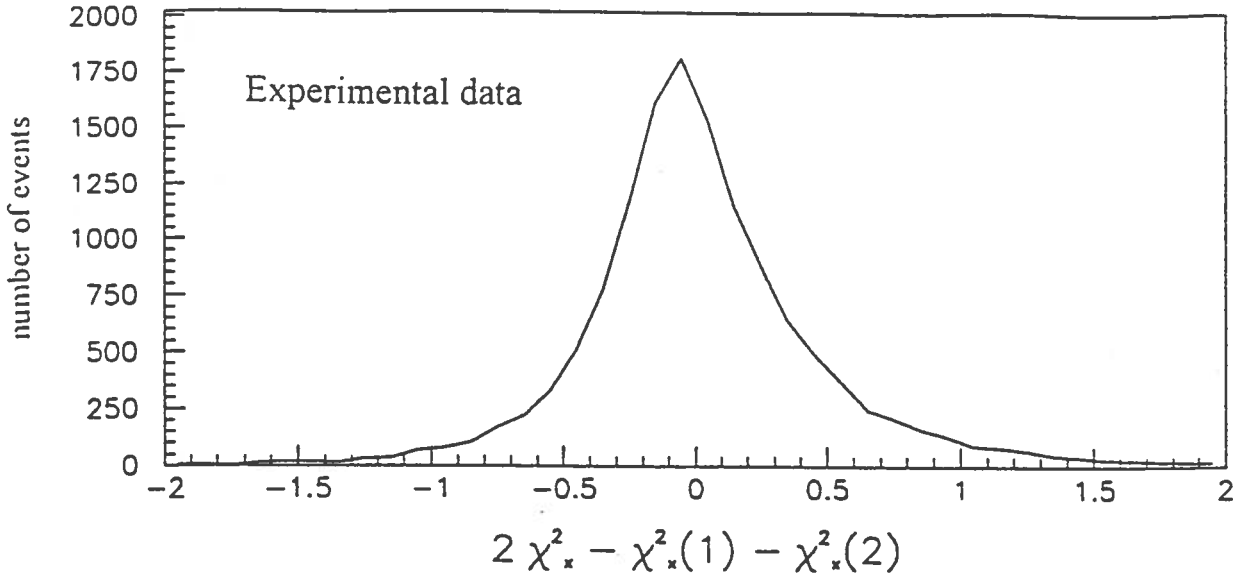

8-a

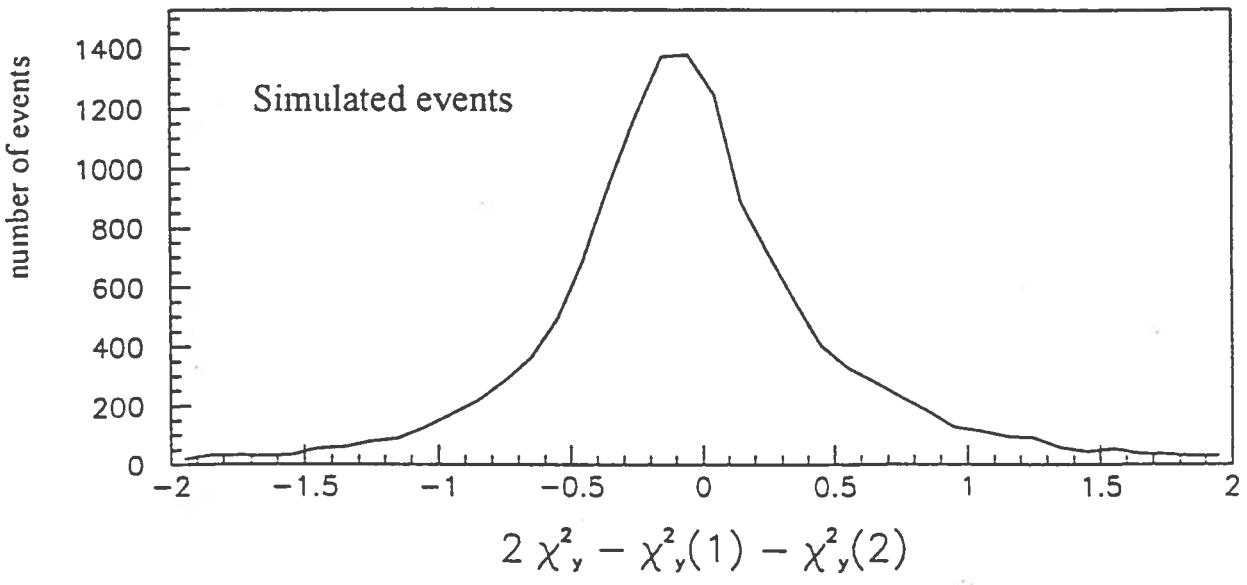

8-b

Figure 8. Distribution of the difference $2\chi^2_x$-$\chi^2_x(1)$-$\chi^2_x(2)$ for the helium sample of the MASS-91 flight (8-a). The corresponding distribution of the helium events generated by the Monte Carlo method described in Section 3 is shown in fig. 8-b. The two distributions are normalized to the same number of events.

The average vanishing difference between the $2\chi_y^2$ of the entire trajectory and the sum of the χ_y^2 –values of the 2 parts of the same trajectory, $\chi_y^2(1) + \chi_y^2(2)$, indicates that the track fitting is appropriate. On the contrary, an abnormal difference would signal the presence of elastic nuclear scattering events or other spurious effects.

The deflection η resulting from the full trajectory should agree with the deflections, $\eta(1)$ and $\eta(2)$, of the two separated segments of the trajectory. In an ideal case, the result should be $\eta(1)=\eta(2)=\eta$. Good-quality trajectories are expected to exhibit $\eta(1)\approx\eta(2)\approx\eta$ within the accuracy of the measurement errors. Figure 9-a shows the distribution of the difference $[\eta(1)-\eta(2)]/\eta$ for a cosmic helium sample of 11378 events of the MASS-91 flight. The number of events populating the tails of the distribution defined by the inequality $|\eta(1)-\eta(2)|/\eta \geq 4$ are only 188 (1.6 %).

In figure 10 is plotted $\eta(2)/\eta$ versus $\eta(1)/\eta$ for the same helium sample used in fig. 9. If the deflection of the first segment $\eta(1)$ is approximately equal to that of the full trajectory, then the ratio $\eta(1)/\eta$ should cluster around 1. A similar behavior is expected for the ratio $\eta(2)/\eta$. Thus, the zone around the point with the coordinate pair $\eta(1)/\eta= \eta(2)/\eta=1$ is expected to be populated by events with a correct curvature measurement. As an example, the event fraction inside the circumference with a radius of 2 and centered in the coordinate pair $\eta(1)/\eta= \eta(2)/\eta=1$ is 86%. Helium trajectories with well-measured curvatures populate this circle.

The results in figures 7, 8, 9 and 10 are typical of genuine helium events. The shapes and standard deviations of these distributions are peculiar of the MASS spectrometer and set the standard for helium or antihelium identification criteria.

5. Curvature misidentification probability in a cosmic-ray helium sample

It is interesting to study an event sample where the curvature sign of cosmic helium measured by the tracking system shown in fig. 2 is incorrect. The incorrectness in the curvature sign is postulated on the basis of the negative experimental evidence in the quest of genuine cosmic antihelium, determined by all experiments made until the present date [17-29].

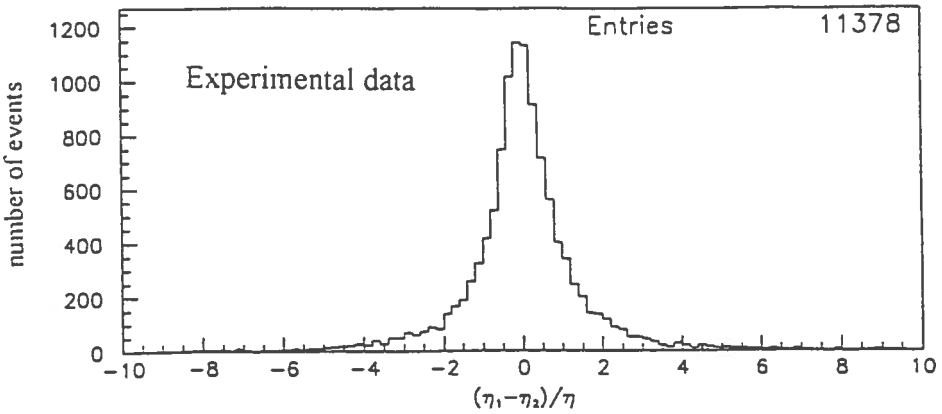

9-a

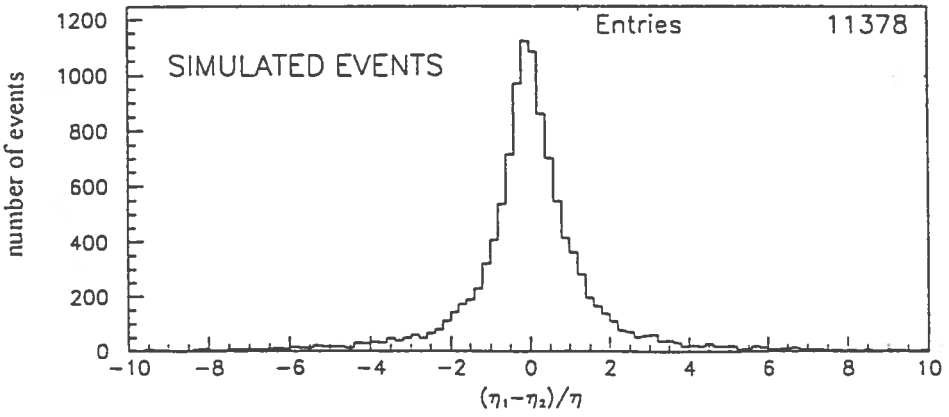

9-b

Figure 9. Distribution of the relative difference in the deflections | η(1) - η(2) | / η for a sample of 11378 helium events of the MASS-91 flight surviving the trajectory cuts described in Section 3 (9-a). The corresponding distribution generated by the Monte Carlo method, filtered by the same trajectory cuts, is shown in fig. 9-b.

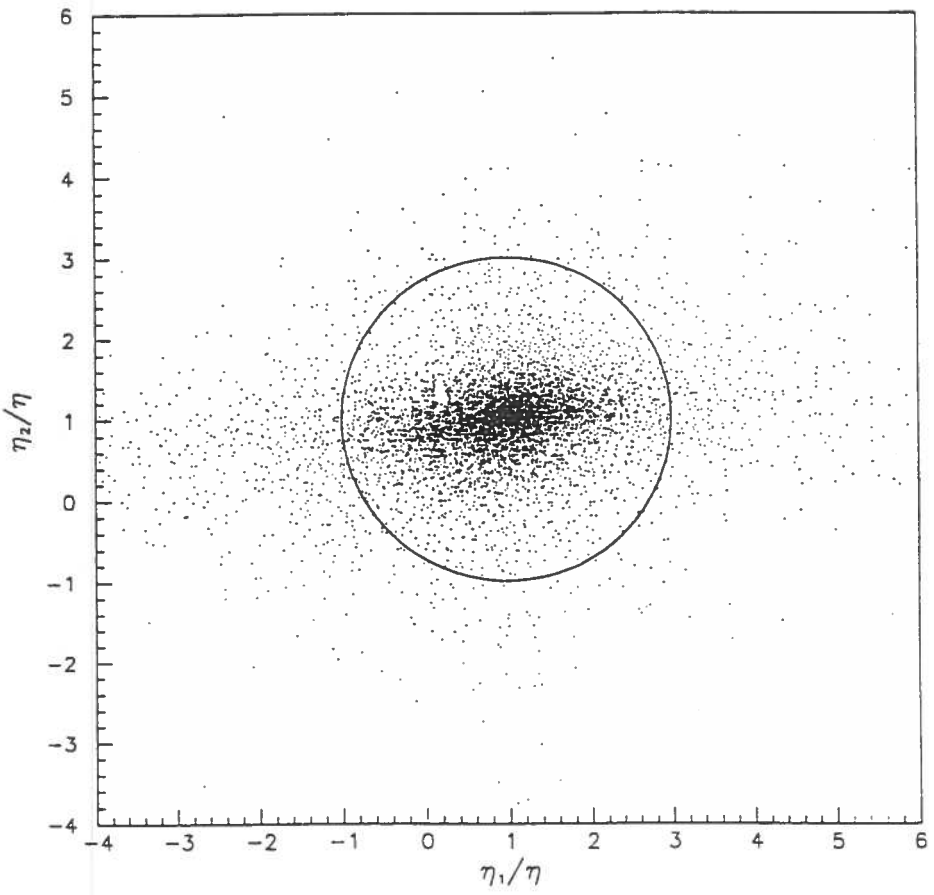

Figure 10. $\eta(1)/\eta$ versus $\eta(2)/\eta$ for a cosmic helium sample of the MASS-91 flight. The clustering of the events around the coordinate pair $\eta(1)/\eta = \eta(2)/\eta = 1$ indicates that the event sample has well-measured curvatures. The data points inside the circle are a fraction of 0.86 of the entire sample.

The deflection distribution of a cosmic helium sample surviving the helium selection criteria given in Section 3 is shown in figure 11-a. The trajectory cuts (α), (β), (γ), (δ) and (ε) given in Section 3.3 are not applied to this data sample. The deflection distribution in a magnified negative interval (i.e. events appearing in the spectrometer with negative curvatures) is shown in figure 11-b.

Thus, according to the *a priori* assumption mentioned above, all trajectories in fig. 11-b have incorrect curvature measurements. Looser trajectory cuts used to select cosmic antiprotons [5], primary positrons [14], muons and pions [15] and other particles [16] in the MASS spectrometer are inadequate to reject all the negative curvatures of the helium sample when the number of events exceeds about 10^5 events as discussed in Section 3. The study of elastic nuclear scattering of helium in the matter layers of the tracking system made in Sections 3 and 4 suggests the appropriate ranges of those parameters which discriminate between correct and incorrect measurements of curvature.

On the basis of the results given in Section 4, the intervals in the values of η and χ^2 for the full track and the two segments of the same track are the following:

(A) $\quad |\, 2\chi^2_x - \chi^2_x(1) - \chi^2_x(2)\,| \le 0.8$

(B) $\quad |\, 2\chi^2_y - \chi^2_y(1) - \chi^2_y(2)\,| \le 0.8$

(C) $\quad |\, \eta(1) - \eta(2)\,| \,/\, \eta \le 4$

(D) $$\left(\frac{\eta(1)}{\eta} - 1\right)^2 + \left(\frac{\eta(2)}{\eta} - 1\right)^2 = 4$$

The conditions (A) and (B) require that the 6 χ^2-values of the full track and those of the two track segments are consistent within the statistical fluctuations expected for genuine events. The criterion (C) requires that the relative difference in the two deflections of the separated trajectories do not exceed the value of 4 as suggested by the experimental data shown in fig. 9. The last criterion (D) ensures that the curvature signs of the two track segments are consistent with that of the full track within the measurement errors.

The set of cuts (A), (B), (C) and (D) will be referred to as curvature cuts. They have been conceived to identify the correct curvatures of helium trajectories.

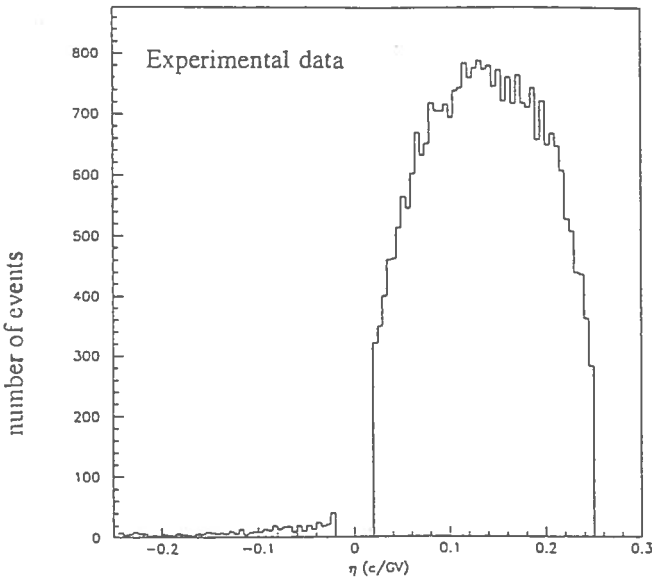

11-a

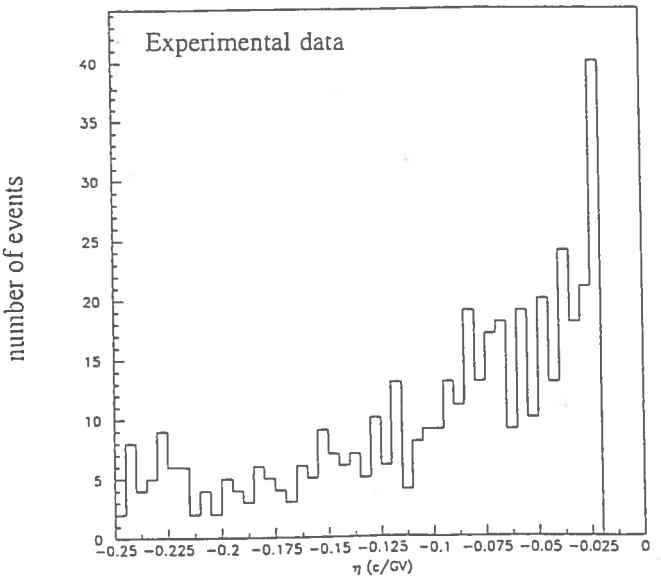

11-b

Figure 11. Deflection distribution of the helium sample selected by pulse amplitudes in the scintillator counter system used in the MASS-91 flight (11-a). In the expanded scale of fig. 11-b only the negative deflection distribution is shown. This kind of events, peculiar of a given spectrometer, forms an insidious background to be identified and rejected in the quest of cosmic antihelium.

In order to identify those helium events suffering elastic nuclear scatterings and inducing a curvature misidentification, we have calculated by Monte Carlo technique the corresponding 4 distributions of the variables: $2\chi^2_x-\chi^2_x(1)-\chi^2_x(2)$, $2\chi^2_y-\chi^2_y(1)-\chi^2_y(2)$, $[\eta(1)-\eta(2)]/\eta$ and, finally, $\eta(1)/\eta$ versus $\eta(2)/\eta$.

Any significant deviations of these 4 distributions from those obtained in the analysis of the experimental data (in figures 8-a, 9-a, 10 and 11) may be utilized to label and remove scattering events. For example, the computed discrimination power of the variable $2\chi^2_x-\chi^2_x(1)-\chi^2_x(2)$ against elastic nuclear scattering is illustrated by the curve shown in figure 12, which gives the ratio $[2\chi^2_x-\chi^2_x(1)-\chi^2_x(2)]_{scatt}/[2\chi^2_x-\chi^2_x(1)-\chi^2_x(2)]_{reg}$ as a function of $[2\chi^2_x-\chi^2_x(1)-\chi^2_x(2)]_{reg}$, where this last variable refers to regular events and $[2\chi^2_x-\chi^2_x(1)-\chi^2_x(2)]_{scatt}$ to scattering events.

Figure 13 shows the distribution $\eta(2)/\eta$ versus $\eta(1)/\eta$ for a simulated helium sample suffering elastic nuclear scatterings. Both trajectory and curvature cuts are applied in this simulation with the only exception of the χ^2-cut that has been set at the value of 4 instead of 2.5. This looser cut allows a larger number of events in fig. 13 to survive. The different clustering of the elastic nuclear scattering events in the plane $\eta(2)/\eta$ versus $\eta(1)/\eta$ with respect to that displayed by the experimental data shown in fig. 10 shows the powerful discrimination between regular and scattering events that is achievable by selecting the appropriate zone in this plane.

Due to the long computer time needed for the trajectory reconstruction, several sets of simulated helium samples, each of 10^5 events, have been regarded as adequate for our background estimate.

When the curvature cuts are applied to the various simulated subsamples of 10^5 helium events which have undergone elastic nuclear scattering and survived the trajectory cuts of the MASS spectrometer given in Section 3.3, only an average number of 8 ± 3 events are left. This result leads to the following background estimate for the genuine antihelium signal in the MASS spectrometer. Since a sample of 10^5 helium events undergoing elastic nuclear scattering corresponds to a sample of $1.48^{+0.25}_{-0.18} \cdot 10^7$ events, it turns out that the probability of observing one misidentified helium curvature is $5.4^{+3.0}_{-2.5} \cdot 10^{-7}$ in the momentum band 8-100 GeV/c.

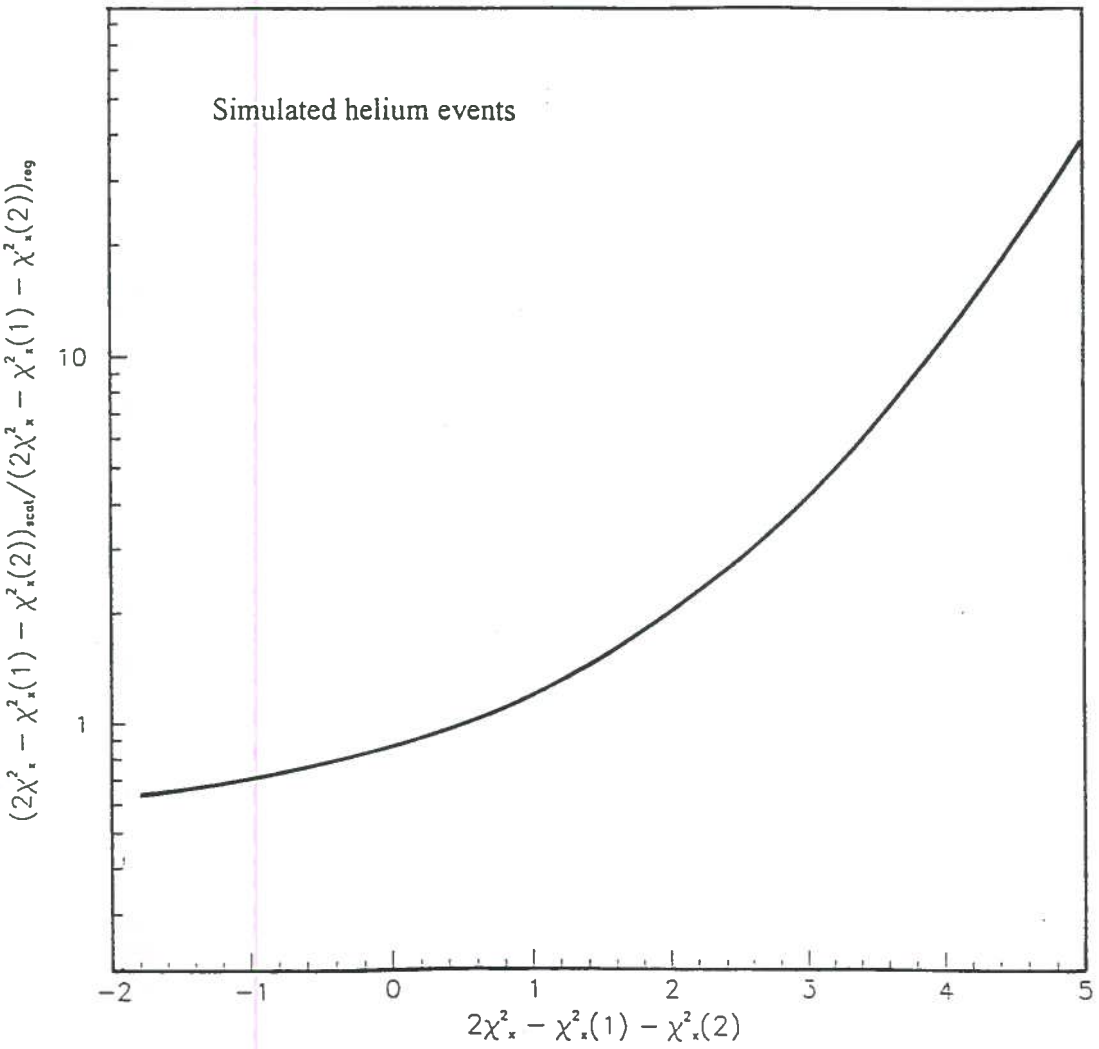

Figure 12. Ratio between the quantity $2\chi^2_x$-$\chi^2_x(1)$-$\chi^2_x(2)$ for 100000 simulated helium events suffering elastic nuclear scatterings and the same quantity for 100000 regular events. The observed increasing ratio demonstrates that scattering events may be rejected by a suitable cut in the variable $2\chi^2_x$-$\chi^2_x(1)$-$\chi^2_x(2)$.

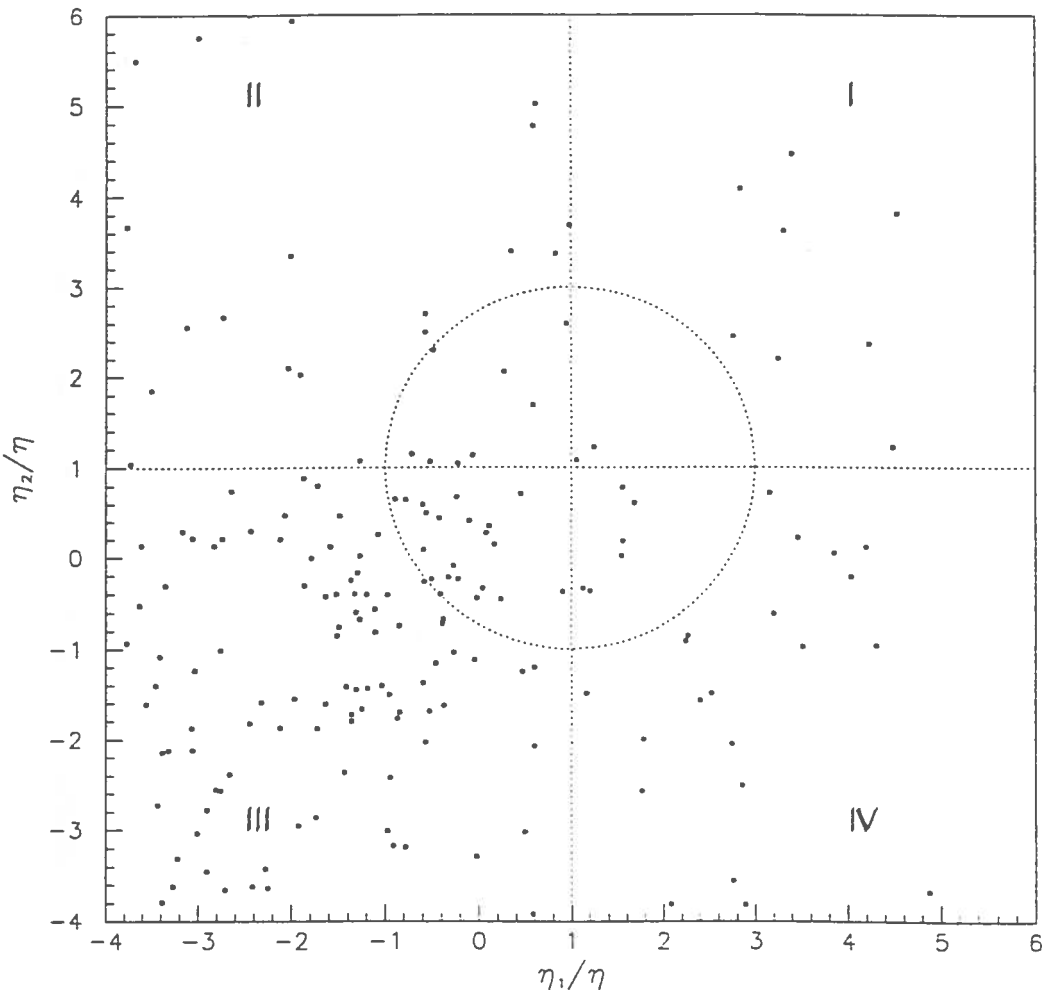

Figure 13. $\eta(2)/\eta$ versus $\eta(1)/\eta$ for a simulated sample of 100000 helium events that has undergone elastic nuclear scatterings and survived the trajectory cuts (see Section 3) except for the χ^2-values which, in this specific simulation, satisfy the inequalities $\chi^2_x \leq 4$ and $\chi^2_y \leq 4$.

The total event sample collected with the instrument flown in Fort Sumner, New Mexico in 1991 and 1993 surviving the helium selection criteria given in Section 3.3 amounts to 76346 events. Therefore, the corresponding number of fake antihelium events due to curvature misidentification surviving both the trajectory and the curvature cuts is $0.041\,^{+0.023}_{-0.019}$ events. This estimated number of background events assumes that the elastic nuclear scattering is the dominant process generating fake antihelium. This hypothesis is substantiated by the results displayed in fig. 6 where no events out of 200000 fully reconstructed trajectories of regular events survive the cut $|\eta|/\sigma_\eta>5$ and further corroborated by the results of a previous study (see Section 7 of ref. 6).

6. Quality factor in the curvature measurement

When the accuracy in the deflection measurement $|\eta|/\sigma_\eta$ increases, the number of helium events appearing with negative deflection decreases as shown in fig. 6. Thus, it is interesting to determine the dependence of the fraction of helium events with incorrect curvatures, w_c, on the accuracy of the deflection measurement. The quantity w_c is evaluated by counting the fraction of events with opposite curvature signs between the deflection of the full trajectory and those of the two track segments. The quantity w_c as a function of $|\eta|/\sigma_\eta$ for an experimental helium sample is shown in figure 14. Most of these events populate the quadrant denoted by III in fig. 13 where the distribution $\eta(2)/\eta$ versus $\eta(1)/\eta$ is reported. When the ratio $|\eta|/\sigma_\eta$ improves by a factor of 2 going, for example, from 5 to 10, the number of events with inconsistent curvature sign decreases by a factor of 8. The curve in fig. 14 can be utilized to calculate the probability that a single helium event with an observed value of $|\eta|/\sigma_\eta$ has an incorrect curvature sign because of the limited accuracy in the deflection measurement of the spectrometer. For example, the probability of observing an incorrect curvature sign of an event with $|\eta|/\sigma_\eta=30$ is 10^{-6}. In this crude estimate, a constant slope of the dashed curve in fig. 14 has been assumed at values larger than 20.

An interesting circumstance arises by studying the data reduction of the two MASS flights resulting from the application of the curvature cuts to the helium sample surviving the trajectory cuts enumerated in Section 3.

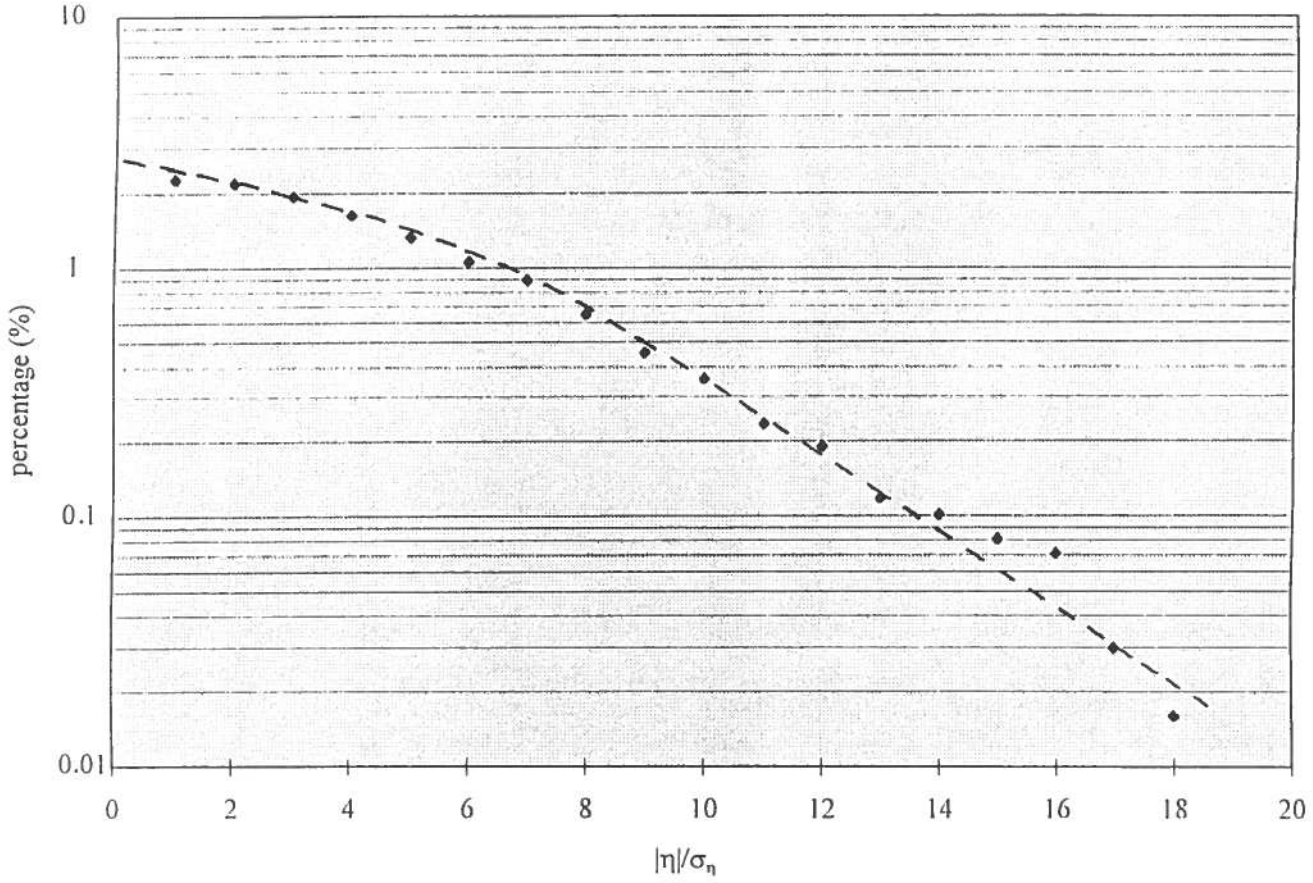

Figure 14. Fraction of helium events with inconsistent curvature sign as a function of the accuracy in the deflection measurement, $|\eta|/\sigma_\eta$, for the MASS-91 flight. The dashed curve is an interpolation of the data.

The values of important parameters of the 2 events with negative deflections surviving the curvature cuts and therefore appearing in the spectrometer as antihelium events are given in Table I.

Table I

Parameters of the 2 events surviving the curvature cuts in a data sample of 76346 events with $|Z|=2$.

	Event E_1 number 600973 MASS-91	**Event E_2** number 2082343 MASS-93
χ^2-values		
χ^2_x	0.476	0.678
χ^2_y	0.761	0.655
Momentum (GeV/c) and deflection accuracy		
momentum	30.4±2.5	11.2±0.3
deflection accuracy $\lvert\eta\rvert/\sigma_\eta$	12.2	39.1
Curvature sign		
full track	negative	negative
first segment	negative	negative
second segment	negative	negative

The 2 events surviving the curvature cuts have excellent values of the parameters specifying their trajectories and they fail the hypothesis of genuine cosmic helium undergoing elastic nuclear scattering in the spectrometer. The reconstructed trajectories in the maximum bending plane of the spectrometer of the 2 events are shown in figure 15.

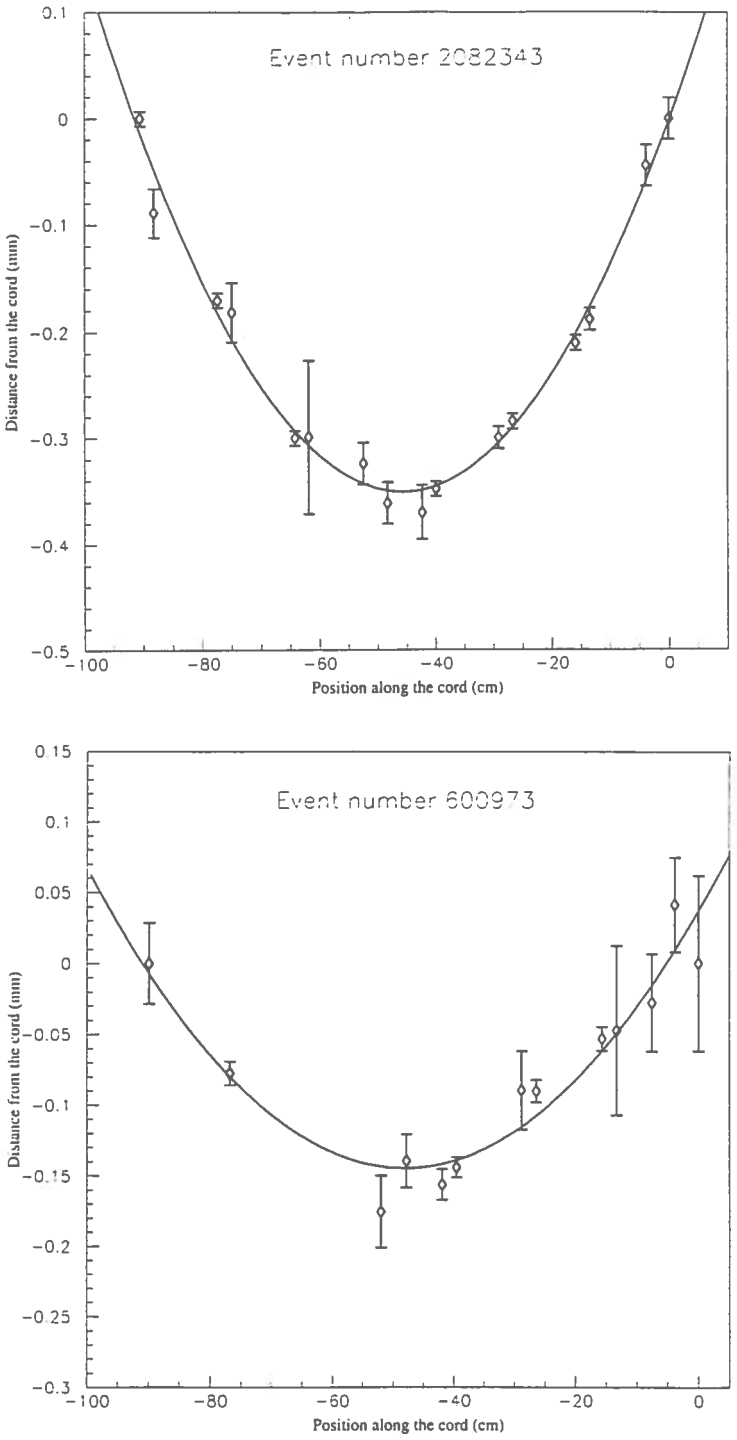

Figure 15. Projected trajectories in the maximum bending plane of the spectrometer of the 2 events with negative curvature and |Z|=2 surviving all the selection criteria applied to reject misidentified helium curvatures. The trajectories are given in the reference frame specified in fig. 4-a where the two extreme coordinates of the trajectory define the cord (horizontal axis in this figure 15). Note the different length unit for abscissae and ordinates. The solid line is a parabolic fit through the position measurements.

7. Conclusions

A study of the parameters affecting the curvature measurements in magnet spectrometers has been reported. The results of this study are based on Monte Carlo simulation and on the analysis of experimental data in the helium rigidity interval 4-50 GV/c.

The simulation of the MASS spectrometer indicate that the probability of observing helium events with negative curvature (fake antihelium events) is $1.75 \cdot 10^{-6}$ when the trajectory cuts on the track quality are applied to the experimental data. This probability decreases to the value of $5.4 \cdot 10^{-7}$ if additional requirements (curvature cuts) on the track quality are imposed. Curvature cuts have been conceived to reject events that have suffered elastic nuclear scatterings in the spectrometer.

A good agreement between the average properties of the simulated events and those of the experimental data has been found at every step of this study. However, two helium events with negative curvature survive both the trajectory and curvature cuts. The assessment of the nature of these 2 events and its implication in Astrophysics is beyond the perimeter of this paper.

All the experiments that searched for antinuclei in the primary cosmic radiation since 1961 are listed in Table II. The outcome of these experiments is in the form of upper limits of antinucleus-to-nucleus flux ratios, also given in the same Table II. The papers describing these studies lack of a detailed account of how the initial data samples of cosmic rays reduce to zero events.

To our knowledge, this study presents, for the first time, a quantitative analysis of data reduction versus selection criteria in a magnet spectrometer searching for antinuclei and may both facilitate and stimulate a critical comparison of the experimental results of present and future experiments.

Table II

Upper limits to the antinucleus-nucleus flux ratios in the primary cosmic radiation determined by cosmic ray experiments in the period 1961-1997.

Atomic Number |Z|	Rigidity range (GV/c)	Number of events	Upper limits on the flux ratios	Experiment
2	1.3-2.7	500	$7 \cdot 10^{-3}$	Aizu et al. (1961)
	1.2-10.4	2189	$1.4 \cdot 10^{-3}$	Evenson (1972)
	10-25	40	$8 \cdot 10^{-2}$	Evenson (1972)
	14-100	116	10^{-2}	Verma et al. (1973)
	4-33	6300	$5 \cdot 10^{-4}$	Smoot et al. (1975)
	33-100	180	$2 \cdot 10^{-2}$	Smoot et al. (1975)
	4-33	$2.3 \cdot 10^{4}$	10^{-4}	Badhwar et al. (1978)
	33-100	100	10^{-2}	Badhwar et al. (1978)
	1-1.8	Not given	$2.2 \cdot 10^{-5}$	Buffington et al. (1981)
	1-19	$11.43 \cdot 10^{5}$	$8 \cdot 10^{-6}$	Ormes et al. (1995)
	0.6-15	$2.065 \cdot 10^{5}$	$4.4 \cdot 10^{-5}$	Anraku et al. (1996)
	1-25	$4.2 \cdot 10^{4}$	$9 \cdot 10^{-5}$	Golden et al. (1997)
	1.6-19	$5.36 \cdot 10^{5}$	$8.1 \cdot 10^{-6}$	Ormes et al. (1997)
≥ 3	<3	442	$2 \cdot 10^{-2}$	Grigorov et al. (1964)
	<4	352	$2 \cdot 10^{-2}$	Ivanova et al. (1968)
	4-125	416	$5 \cdot 10^{-3}$	Golden et al. (1974)
	4-33	$4.1 \cdot 10^{4}$	$8 \cdot 10^{-5}$	Smoot et al. (1975)
	3-100	560	$6 \cdot 10^{-3}$	Smoot et al. (1975)
≥ 6	1.3-2.7	300	10^{-2}	Aizu et al. (1961)
	10-18	40	$7 \cdot 10^{-2}$	Greenhill et al. (1971)
≥ 9	2-20	$2.04 \cdot 10^{4}$	$1.5 \cdot 10^{-4}$	Lund and Rotenberg (1986)

Acknowledgments

We express out gratitude to François Plouin of Laboratoire National de Saturne at Saclay (France) for enlightening discussions about helium-nucleus cross sections.

References

[1] Buffington A. et al. 1981, The Astrophysical Journal, **248**, 1179-1193.

[2] Ormes J.F. et al. 1995, Proceedings of the XXIV ICRC Rome, **Vol. 3**, 92-95.

[3] Codino A. and Lanfranchi M. 1997, The Astrophysical Journal, **487**, 217-224.

[4] Golden R.L. et al. 1984, Astrophysical Letters **24**, 75-83.

[5] Hof M. et al. 1996, The Astrophysical Journal, **467**, L23-L26.

[6] Golden R.L. et al. 1991, Nuclear Instruments and Methods in Physics Research A, **306**, 366-377.

[7] Ahlen S.P et al. 1982, The Astrophysical Journal, **260**, 20-32.

[8] Hof M. et al. 1994, Nuclear Instruments and Methods in Physics Research A, **345**, 561-569.

[9] Ableev V.G. et al. 1991, Zeitschrift für Physik, A**3**, 191-197.

[10] Morsch H.P. et al. 1994, Zeitschrift für Physik, A **350**, 167-169.

[11]Ableev V.G. et al. 1985, Acta Physica Polonica, vol. B **16**, 913-929.

[12] Franco V. and Varma G.K. 1978, Physical Review C, vol. **18**, 349-370.

[13] Codino A. et al. 1997, Conference Proceedings of the Vulcano Workshop 1996, 447-454, Published by the Italian Physical Society.

[14] Golden R.L. et al. 1996, The Astrophysical Journal, **457**, L103-L106.

[15] Brunetti M.T. et al. 1996, Journal of Physics G: Nucl. Part. Phys., **22**, 145-153.

[16] Codino A. et al. 1997, Journal of Physics G: Nucl. Part. Phys., **23**, 1751-1763.

[17] Aizu H. et al. 1961, Physical Review, **121**, 1206-1217.

[18] Badhwar G.D. et al. 1978, Nature, **274**, 137-139.

[19] Evenson P. 1972, The Astrophysical Journal, **176**, 797-808.

[20] Golden R.L. et al. 1974, The Astrophysical Journal, **192**, 747-751.

[21] Verma R.P. et al. 1972, Nature Physical Science, vol. **240**, 135-137.

[22] Greenhill J.G. et al. 1971, Nature, **230**, 170-172.

[23] Grigorov N.L. et al. 1964, Soviet Phys. JETP, **18**, 272-273.

[24] Ivanova N.S. et al. 1968, Cosmic Research, **66**, 69-72.

[25] Lund N. and Rotenberg M. 1986, Astronomy & Astrophysics, **164**, 231-236.

[26] Smoot G.F. et al. 1975, Physical Review Letters, **35**, 258-261.

[27] Anraku K. et al. 1996, KEK Report 96-12.

[28] Golden R.L. et al. 1997, The Astrophysical Journal, **479**, 992-996.

[29] Ormes J. F. et al. 1997, The Astrophysical Journal, **482**, L187-L190.